

# Normalized Steepness Index along the Himalayan Arc as a proxy for Indian plate segmentation

Raj Sunil Kangregula<sup>1</sup>, Pavankumar Gayatri<sup>2</sup>, and Ajai Manglik<sup>1</sup>

<sup>1</sup>CSIR-National Geophysical Research Institute

<sup>2</sup>National Geophysical Research Institute

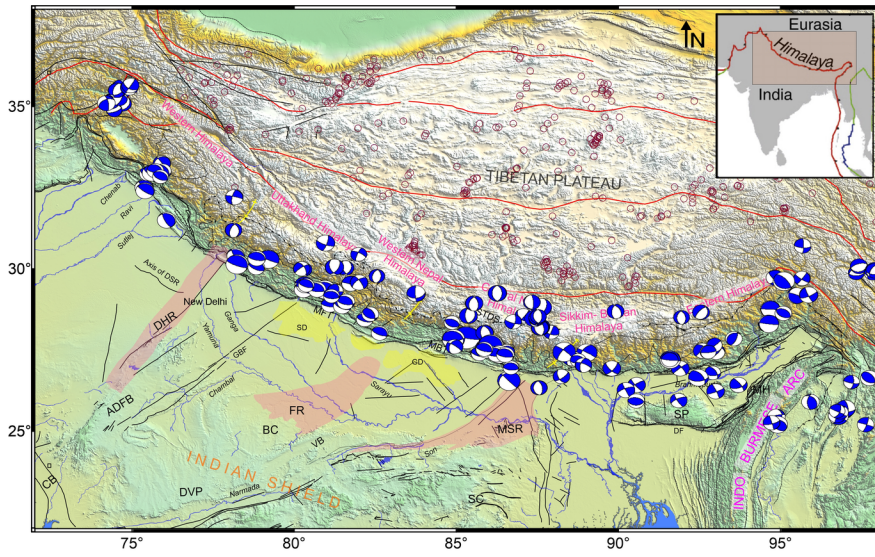
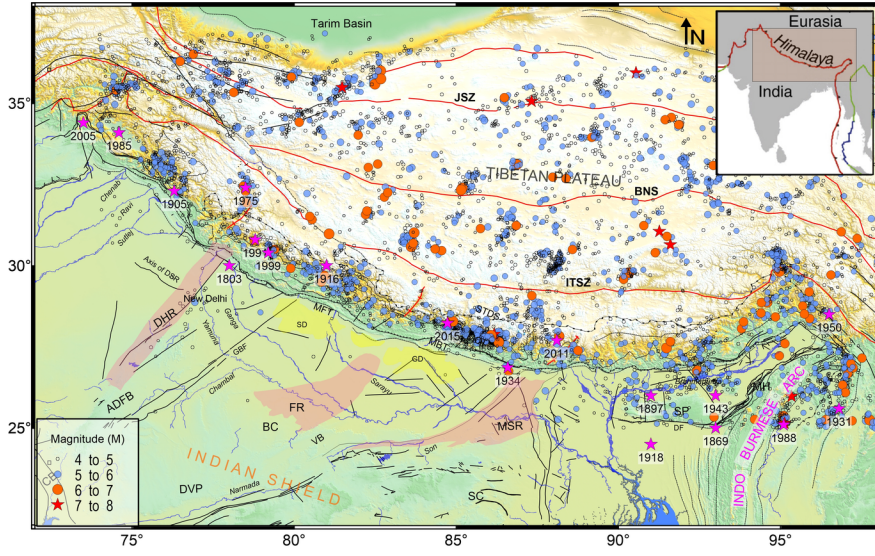
December 13, 2022

## Abstract

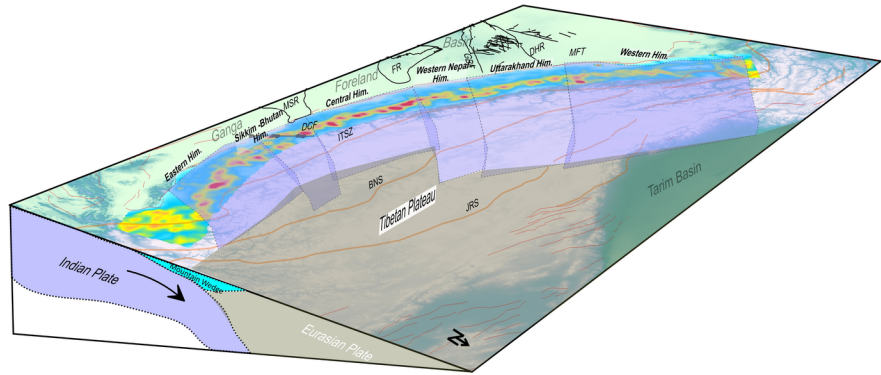
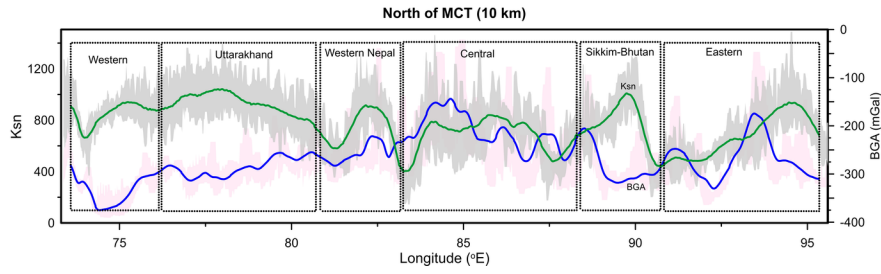
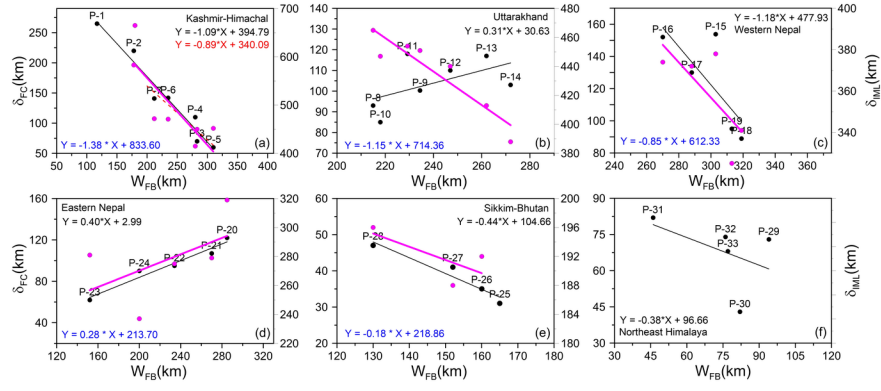
The Indian plate underthrusting the Himalaya is considered to be segmented along the collision belt arc and seismic images of the Indian mantle lithosphere (IML) suggest along-arc variations in the angle of underthrusting and its northern limit beneath Tibet. The pre-existing transverse tectonic structures of the Indian plate mapped in the Ganga foreland basin have been related to these segmentation boundaries. These segmentations imply changes in mechanical properties of adjoining blocks which should manifest in the form of spatial variations in topography build-up. We have analysed a geomorphic index, normalized channel steepness (ksn), along the Himalayan arc using the ALOS elevation dataset to test whether there is any correlation between the and these segmentation boundaries. Our results bring out spatial variability in the along the arc. Based on these results, the arc can be segmented into five blocks, similar to the ones delineated based on correlation between the width of the Ganga foreland basin and the disposition of major Himalayan thrusts from the foothills. Thus, the can be used as a proxy to demarcate different tectonic blocks along the Himalayan arc. Further, we have found a good correlation between the basin width and the northern limit of the IML for all block except the Uttarakhand block. We infer that transverse crustal heterogeneities in this block due to the continuation of different litho-units of the Aravalli-Delhi Fold Belt could be a plausible cause for this anti-correlation.

## Hosted file

951742\_0\_art\_file\_10522156\_rmmlcj.docx available at <https://authorea.com/users/565844/articles/612716-normalized-steepness-index-along-the-himalayan-arc-as-a-proxy-for-indian-plate-segmentation>







1 **Normalized Steepness Index along the Himalayan Arc as a proxy for**  
2 **Indian plate segmentation**

3 Raj Sunil Kandregula, Pavankumar, G\*., Manglik, A.

4 CSIR-National Geophysical Research Institute, Uppal Road, Hyderabad – 500 007, INDIA

5

6 **Corresponding Author:**

**Dr. G. Pavankumar**

Room Nr. 113, Main Building

CSIR-National Geophysical Research Institute

Uppal Road, Hyderabad – 500007, INDIA.

Tel. : +91-40-27012884

Fax. : +91-40-23434651

Email: [gayatripavan@ngri.res.in](mailto:gayatripavan@ngri.res.in)

[Pavan.ngri@gmail.com](mailto:Pavan.ngri@gmail.com)

7

8

9

10

11

12

13

14

15

16

17

18

19

20

21

## 22 **Abstract**

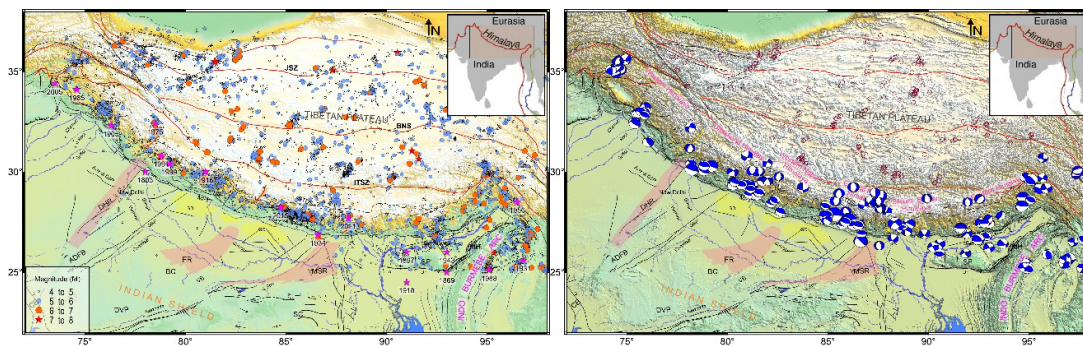
23 The Indian plate underthrusting the Himalaya is considered to be segmented along the  
24 collision belt arc and seismic images of the Indian mantle lithosphere (IML) suggest along-  
25 arc variations in the angle of underthrusting and its northern limit beneath Tibet. The pre-  
26 existing transverse tectonic structures of the Indian plate mapped in the Ganga foreland  
27 basin have been related to these segmentation boundaries. These segmentations imply  
28 changes in mechanical properties of adjoining blocks which should manifest in the form of  
29 spatial variations in topography build-up. We have analysed a geomorphic index, normalized  
30 channel steepness ( $k_{sn}$ ), along the Himalayan arc using the ALOS elevation dataset to test  
31 whether there is any correlation between the  $k_{sn}$  and these segmentation boundaries. Our  
32 results bring out spatial variability in the  $k_{sn}$  along the arc. Based on these results, the arc  
33 can be segmented into five blocks, similar to the ones delineated based on correlation  
34 between the width of the Ganga foreland basin and the disposition of major Himalayan  
35 thrusts from the foothills. Thus, the  $k_{sn}$  can be used as a proxy to demarcate different  
36 tectonic blocks along the Himalayan arc. Further, we have found a good correlation between  
37 the basin width and the northern limit of the IML for all block except the Uttarakhand block.  
38 We infer that transverse crustal heterogeneities in this block due to the continuation of  
39 different litho-units of the Aravalli-Delhi Fold Belt could be a plausible cause for this anti-  
40 correlation.

## 41 **1. Introduction**

42 Collision of the Indian plate with the Eurasian plate around ~55 Ma resulted in the formation  
43 of the ~2500 km long Himalayan mountain belt and the highest-altitude Tibetan Plateau on  
44 earth (Molnar and Tapponnier, 1975, Patriat and Achache, 1984). This vital process which  
45 shortens the lateral spreading of the Indian lithosphere, has been ongoing since then  
46 (Bilham et al., 1998; Avouac, 2003) and it is also conspicuous from the convergence along  
47 the Himalayan arc, Tibetan plateau due to the eastward rise of the earth's crust and  
48 southward transposition at the eastern syntaxes (Molnar and Lyon Caen, 1989; Wang et al.,  
49 2001; Zhang et al., 2004). This convergence is somewhat captivated by the shortening of the  
50 underthrusting Indian plate below the Tibetan plate and also consumed part of it by the  
51 Tibetan Plateau (Li and Song, 2018; Parsons et al., 2020). The inter-continental  
52 convergence between India and Eurasia has led to the generation of several strain zones,  
53 thrusts, highly fractured and jointed rock formations in the Himalayan terrain which caused  
54 instability due to seismic activity. Recent studies on the Himalayan deformation suggest that  
55 the southern Tibet has advanced towards India by sliding over the top of the underthrusting

56 Indian plate at a rate of ~16-18 mm/yr (Ghavri and Jade, 2021; Dal Zilio et al., 2020). This  
 57 has resulted in piling up of the slip deficit and stresses at the northern stretch of the MHT  
 58 which is currently locked to the Indian plate by friction at its base. About 10-20 mm/yr of  
 59 varying shortening rates is suggested for the Himalayan arc from Nanga Parbat (west) to  
 60 Namcha Burwa (east) (Jade et al., 2004).

61 The enduring convergence between the two tectonic plates generated several  
 62 devastating earthquakes in the entire Himalayan arc since historical past making this region  
 63 as one of the most seismically active regions of the world. The Himalayan orogenic belt has  
 64 been struck by several devastating earthquakes in the past (Figure 1) viz., 1897 Shillong  
 65 (Mw > 8), 1905 Kangra (Mw 7.8), 1934 Bihar-Nepal (Mw > 8), 1950 Tibet-Assam (Mw 8.6),  
 66 2005 Kashmir (Mw 7.6), 2015 Gorkha (Nepal, Mw 7.8) (Rajendran and Rajendran, 2005;  
 67 Bilham, 2019). A number of geophysical investigations have been conducted across the  
 68 Himalayan mountain belt to image the geometry of the MHT and its variations in different  
 69 tectonic domains/segments of the collision zone and lithospheric structure that enhances the  
 70 understanding of the ongoing orogenic evolution and earthquake genesis (Lyon-Caen and  
 71 Molnar, 1985; Brown et al., 1996; Nelson and Zhao et al., 1996; Zhao et al., 1993; Hauck et  
 72 al., 1998; Tiwari et al. 2006; Wittlinger et al., 2009; Nábělek et al., 2009; Acton et al., 2011;  
 73 Nelson et al., 1996; Brown et al., 1996; Caldwell et al., 2013; Mahesh et al., 2013,  
 74 Pavankumar et al., 2014, Pavankumar and Manglik, 2021).



75

76 **Figure 1.** (a) Map showing seismicity distribution along the Himalayan arc (Source:  
 77 European-Mediterranean Seismological Centre (EMSC) catalogue:1970-2022) and (b) focal  
 78 mechanism of some of the earthquakes along the mountain belt. The fault plane solutions  
 79 are taken from <https://www.globalcmt.org/CMTsearch.html>. The abbreviations are: ADFB –  
 80 Aravalli Delhi fold belt; DVP – Deccan Volcanic Province; VB – Vindhyan Basin; BC –  
 81 Bundelkhand craton; SC – Singhbhum craton; CB- Cambay basin; SP – Shillong Plateau;  
 82 MH – Mikir Hills; DHR – Delhi - Haridwar Ridge; DSR – Delhi - Sargodha Ridge; FR –  
 83 Faizabad Ridge; MSR – Monghyr - Saharsa Ridge; KCR – Kaurik-Chango rift; TR –  
 84 Thankola rift; YR – Yadong rift; GD – Gandak depression; SD – Sharda depression; MFT –  
 85 Main Frontal Thrust; MBT – Main Boundary Thrust; MCT – Main Central Thrust; STDS –  
 86 South Tibetan Detachment System; ITSZ – Indus-Tsangpo Suture Zone; BNSZ – Bangong

87 Nujiang Suture Zone; LSSZ – Longmu Tso Shuanghu Suture Zone; JSSZ – Jinsha Suture  
88 Zone; AKSZ – Anyemaqen Kunlun Suture Zone; DF – Dauki fault.

89 Recent geophysical studies of the collision zone provided evidences of along arc  
90 variations in the Indian lithosphere that has been underthrusting beneath the Tibetan  
91 plateau, in terms of its dip (angle of underthrusting), northern extent of the Indian Mantle  
92 Lithosphere underneath the Tibetan Plateau, lateral variations of the MHT and subduction  
93 geometry through lateral discontinuities in the seismic velocities (Li et al., 2008; Zhao et al.,  
94 2010; Li and Song, 2018), analyses of gravity and elastic properties (Chen et al., 2015; Ravi  
95 Kumar et al., 2020) and by lateral changes in various physical parameters (e.g. Yin, 2006;  
96 Robert et al., 2011). Identifying these segment boundaries is of paramount significance in  
97 seismically active terrains, as these boundaries can confine the dimensions of faulting in a  
98 single earthquake to part of a fraction of the total length of fault, thereby restricting the size  
99 of the earthquake.

100 Segmentation identification studies along the Himalayan arc have been carried out in  
101 various disciplines. Seismological, GPS measurements and correlation between topography  
102 and Bouguer gravity anomaly provided insights for along-arc variations in the crustal-scale  
103 heterogeneities, displacement of the Main Himalayan Thrust (MHT), subducting plate angle  
104 and northward proliferation of the Indian lithosphere into the Himalayan-Tibetan system  
105 (Manglik et al. 2021; Dal Zilio et al. 2020; Bai et al. 2019; Li and Song, 2018; Singer et al.,  
106 2017; Elliott et al. 2016; Zhao et al. 2010). Shaokun et al. (2019) using the P-S wave  
107 velocities ratio advised diverse geometries from west to east for the underthrusting IML.  
108 Further, they contemplated that the slab tear up beneath the eastern Tibet and the  
109 delamination of lithosphere in the western Tibet are the two important factors that can  
110 explain the high  $V_p/V_s$  in the western and decreased  $V_p/V_s$  in the eastern segment of the  
111 Tibetan plateau. Robert et al. (2011) conducted thermochronological studies in the western  
112 and eastern parts of the central Nepal Himalaya and correlated the results with the data of  
113 eastern Nepal and Bhutan Himalaya which highlights the presence of lateral variations in the  
114 geometry of the MHT. They opined that there is no presence of crustal scale MHT ramp in  
115 the western Bhutan and there is a larger dip angle of mid-crustal ramp of the MHT in the  
116 central Nepal rather than in western Nepal

117 Kosarev et al. (1999) highlighted that the Indian lithosphere plunges towards north close  
118 to the Indus-Tsangpo (or Indus-Yarlung) suture and also it is separated from the surface  
119 under the central Tibet. Contrary to this, Tilmann et al. (2003) that the Indian plate  
120 underthrust the Tibetan plateau up to Bangong-Nujiang Suture (BNS), after that it might sink  
121 nearly vertical to at least 400 km depth. Liang et al. (2007) suggested a new tear model in  
122 which the Indian lithosphere is divided into two slabs, a north advancing slab subducting with

123 a steeper angle under the western part and a north-east advancing slab subducting at a  
124 shallower angle under the eastern sector of the Tibetan plateau. Additionally, they suggested  
125 that these two slabs are teared apart along the Yadong-Anduo-Golmund (YAG) tectonic  
126 corridor. Li et al. (2008) suggested that the P-wave travel time tomography unveils  
127 compelling lateral changes in the velocities and estimated the horizontal distance beyond  
128 which the inferred Indian lithosphere drifts northward under the plateau. They proposed that  
129 the IML decreases from west to east. Liang et al. (2012) come up with a new model  
130 suggesting that the segmented Indian slab while underthrusting in the south-central region of  
131 the Tibetan region with compelling lateral physical and compositional variations within the  
132 continental lithosphere.

133 Zhao et al. (2010) observed low-angle subduction of the Indian lithosphere in western  
134 Tibet on the basis of seismic discontinuities and suggested that the subduction angle  
135 gradually becomes steeper towards east. Li and Song (2018) used P and S wave seismic  
136 tomograms and advised that the Indian lithosphere is severed into four major segments with  
137 three main tears along the Himalayan arc with shallow dip angle of subduction towards east  
138 and west compared to the centre. Contrary to this, Dal Zilio et al. (2021) suggested that the  
139 western and eastern blocks have much steeper angles of subduction compared to the  
140 central block by analysing GPS measurements. Hetényi et al. (2016) examined the along-arc  
141 variations using the analysis of arc parallel topography and bouguer gravity anomaly data  
142 and suggested that the three major basement ridges i.e. DHR, FR and MSR played an  
143 important role in the segmentation of the Himalaya into four parts. They further implied that  
144 there is no correlation among the two factors that are considered. Ravi Kumar et al. (2020)  
145 analysed gravity, geoid and elevation data and inferred eastward decrease in the effective  
146 elastic thickness of the Indian lithosphere (58 km in west to the 36 km in east). Mandal et al.  
147 (2015) analysed the long-wavelength topography of the Himalayan hinterland and suggested  
148 the correlation of the varying topography with the along-arc variations in the underthrusting  
149 rate of the Indian plate.

150 Majority of these studies are confined only to the Himalaya-Tibetan region; however, the  
151 formation of the Himalayan Foreland basin and its geometry is also connected with the  
152 dynamics of the underthrusting Indian lithosphere and its pre-orogenic heterogeneities.  
153 Recently, Manglik et al. (2021) tested correlation between the foreland basin width and the  
154 disposition of major thrust faults (distance between MCT and MFT) by using several  
155 topographic and Bouguer gravity anomaly swath profiles crossing the Himalayan arc. The  
156 study inferred a new segmentation boundary which is possibly the extension of the Great  
157 Boundary Fault (GBF) towards north in the vicinity of the Indo-Nepal border separating  
158 Kumaun Himalaya from western Nepal Himalaya.

159 The fundamental objective of tectonic geomorphology is quantitative derivation of tectonic  
 160 and geomorphic indicators from topography. Earth surface process models forecast  
 161 landscape feedback to tectonic forcing whereby topography, erosion rates, and sediment  
 162 production transiently alter to variations in tectonic boundary circumstances (Beaumont et  
 163 al., 1992; Howard et al., 1994; Koons, 1989; Whipple & Tucker, 1999). Analysis of the  
 164 steepness of the mountain belt can provide qualitative information on nature of the  
 165 subsurface and fault segmentation (Kirby and Whipple, 2012). The normalized steepness  
 166 index ( $k_{sn}$ ) is proved to be useful in identifying large scale tectonic deformations (Wobus et  
 167 al., 2006). As the topographic variations within the active margins can be linked to differential  
 168 uplift of the rocks in the region, in the present study we have calculated the  $k_{sn}$  for the  
 169 Himalaya and analysed the along arc variations of the  $k_{sn}$  and integrated the available  
 170 structural variations of the Indian Mantle Lithosphere (IML) to identify possible correlation  
 171 and to understand the related segmentation.

## 172 2. Method and Material:

173

### 174 2.1 Stream power incision model (SPIM): derivation of normalized steepness index

175

176 The Stream Power Incision Model (SPIM) is the most prevalent and frequently used  
 177 technique to model the dynamics of bedrock channel systems (Howard, 1998). The incision  
 178 rate (E) of the river bedrock channel can be represented by the product of erodibility of the  
 179 bed rock (K), drainage area upstream to the river (A) and the topographic slope (S) along the  
 180 river (Howard and Kirby, 1983; Lague, 2013) which is expressed as

181

$$182 \quad E = K A^m S^n \quad (1)$$

183

184 where m and n are positive constants which are associated with basin lithology, hydraulic  
 185 geometry and the erosion process (Snyder et al., 2000; Whipple and Tucker, 2002).

186

187 The detachment-limited mass balance equation affirms that the first order derivative of  
 188 channel elevation (h) in relation to time (t) hinges on the rock uplift rate (U) and incision rate  
 189 (E) (Royden and Perron, 2012; Han et al., 2017) that can be denoted as:

190

$$191 \quad \frac{dh}{dt} = U - E \quad (2)$$

$$192 \quad = U - K A^m S^n \quad (3)$$

193

or

$$194 \quad \frac{dh}{dt} = U(X,t) - K(X,t) A(X,t)^m \left(\frac{dh}{dX}\right)^n \quad (4)$$

195

196 In equilibrium state, the rate of rock uplift is equal to channel incision, i.e.

197

$$198 \quad dh/dt = (U/K)^{1/n} A(X)^{m/n} \quad (5)$$

199

200 Rearranging the above eq. and solving the equation for S under equilibrium conditions gives

201

$$202 \quad S = (U/K)^{1/n} A(X)^{m/n} \quad (6)$$

203 The local channel slope can also be defined by replacing  $(U/K)$  with channel steepness ( $k_s$ )  
204 and  $m/n$  with  $\theta$  (concavity index) which is expressed as

205

$$206 \quad S = k_s A^{-\theta} \quad (7)$$

207

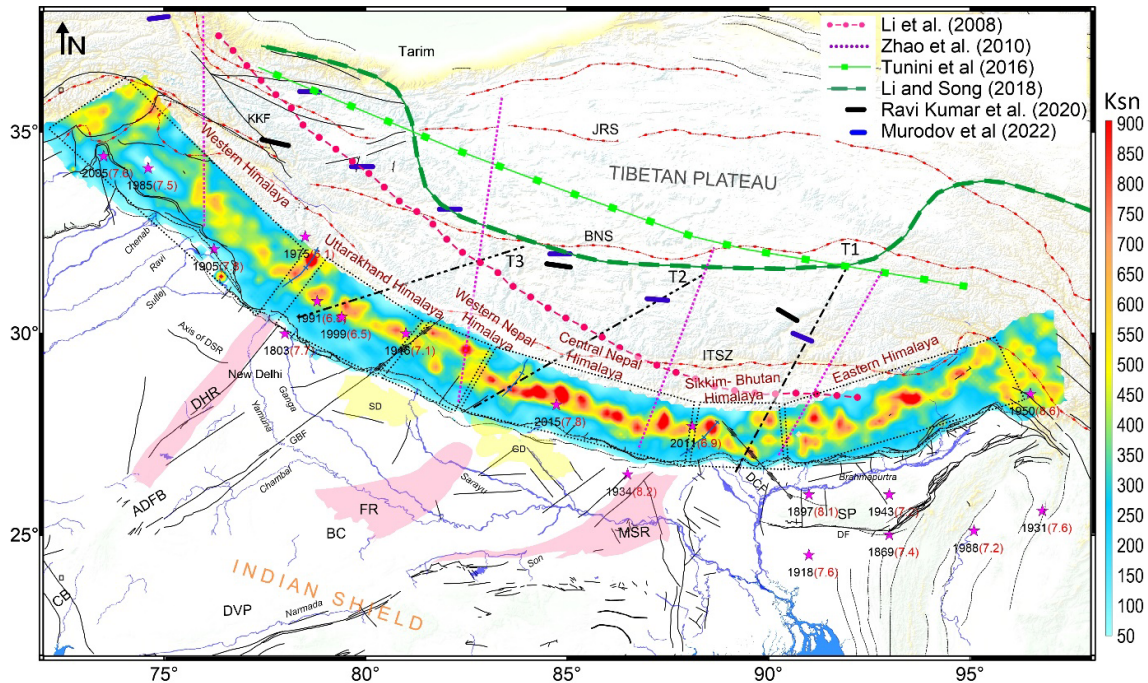
208 In general, the estimation of the concavity index ( $\theta$ ) and steepness index ( $k_s$ ) can be  
209 obtained from the linear regression of gradient against drainage area on a log-log plot (Kirby  
210 and Whipple, 2012). However, little variations or uncertainties in the  $\theta$  (regression slope)  
211 may cause large variations in the steepness index (regression intercept), hence, a  
212 normalized steepness index ( $k_{sn}$ ) is needed to account for this autocorrelation. Thus,  $k_{sn}$  is  
213 evaluated by slope-area regression using a reference concavity index ( $\theta_{ref}$ ), where the  $\theta_{ref}$   
214 of the steady state channels falls in a restricted range of  $0.4 \leq \theta \leq 0.6$ . This permits efficient  
215 correlation of profiles of streams with significantly changing drainage area (Wobus et al.  
216 2006).

217 We analysed all the major streams/rivers which cut across all the major thrust faults along  
218 the 2500 km long Himalayan orogenic belt for the calculation of  $k_{sn}$ . We used Advanced  
219 Land Observing Satellite (ALOS) World 3D (AW3D) Digital Elevation Model (DEM)  
220 (<https://www.eorc.jaxa.jp/ALOS/en/aw3d30/index.htm>) of 30m spatial resolution to extract  
221 the river drainage patterns. The AW3D 30m DEM is very effective especially in mountainous  
222 regions with high slopes and relief (Boulton and Stokes, 2018). Further, the drainage pattern  
223 extracted from this DEM is better in terms of resolution and very closely correlates with the  
224 original drainage pattern compared to the most commonly used DEM's, viz., SRTM and  
225 ASTER (Boulton and Stokes, 2018). The calculation of  $k_{sn}$  was carried out using the topo-  
226 toolbox in MATLAB, where the code was adopted from Schwanghart and Kuhn (2010) and  
227 Schwanghart and Scherler (2014).

228

229 The raw  $k_{sn}$  data obtained were interpolated using the kriging method and the interpolated  
230 data were then subjected to low-pass Gaussian filter of 5 passes. The resultant  $k_{sn}$  contours  
231 are then superimposed on an ALOS AW3D 30m spatial resolution DEM of the Himalayan

232 region (Figure 2). We have superimposed the boundaries of the inferred teared blocks of the  
 233 IML and estimates of northern extent of the IML given by various researchers. The locations  
 234 of the significant earthquakes that occurred in the region are also plotted.



235  
 236  
 237 **Figure 2.** Map showing normalized river steepness index ( $k_{sn}$ ) along the Himalayan arc.  
 238 The northern boundary of the Indian plate proposed by Li et al. (2008), Zhao et al.  
 239 (2010), Tunini et al. (2016), Li and Song (2018), Ravi Kumar et al. (2020) and Murodov  
 240 et al. (2022) are also shown in the figure. Tearing of the Indian lithosphere inferred by Li  
 241 and Song (2018) is shown as dashed lines, T1, T2, T3. Stars indicate the locations of the  
 242 significant earthquakes that occurred in the region. Major geological and structural  
 243 features are taken from the shape files available at the BHUKOSH portal of Geological  
 244 Survey of India (<http://bhukosh.gsi.gov.in/Bhukosh/MapViewer.aspx>). For abbreviations  
 245 please refer Figure. 1.

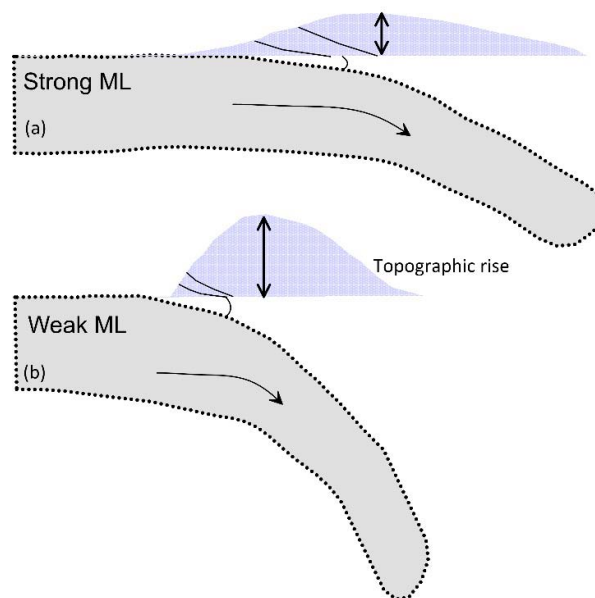
### 246 3. Results and Discussion

247  
 248  
 249 Broadly, the  $k_{sn}$  value ranges between 100 to 1000 with a general eastward increase in its  
 250 value (Figure 2). The central part of the Himalayan arc, i.e., the central and eastern Nepal  
 251 Himalaya region is associated with high  $k_{sn}$  values. The middle portion of the eastern  
 252 Himalaya is also associated with high  $k_{sn}$  values. The detailed discussion on longitudinal  
 253 wise variations of the  $k_{sn}$  for various segments of the arc is presented below.

#### 254 3.1 Western Himalaya (Kashmir and Himachal) (WH, 74 – 78°E longitude)

255 Previously, the region experienced major earthquakes that include 1905 Kangra earthquake  
 256 (M 8.0) and 1985 and 2005 Kashmir earthquakes. The  $k_{sn}$  values of the western Himalaya

257 (till 78°E) are low in comparison to other parts of the collision belt (Figure 2). Here, we  
 258 attempt to explain build-up of topography in terms of strength of the colliding plates. As  
 259 mountain building in a collision belt is linked to flexing of the underthrusting plate and the  
 260 topography load applied on it, it can be understood that a high strength lithospheric plate will  
 261 bend less under a constant applied load, providing a wider area of the plate for horizontal  
 262 movement of the overlying thrust sheets and, thus, less build-up of the steep topography  
 263 (Dahlen, 1990). Conversely, low strength of the plate and large angle of underthrusting shall  
 264 facilitate piling up of thrust sheets giving rise to high topography (Figure 3). Thus, low  $k_{sn}$   
 265 values in this region may be considered as an indication of high strength of the Indian plate  
 266 and low angle of underthrusting plate. This is substantiated by the results showing increased  
 267 northward limit of the Indian mantle lithosphere beneath the Tibetan plateau for this region  
 268 (Li et al., 2008; Li and Song, 2010).



269  
 270 **Figure 3.** Schematic diagram showing relation between strength of the mantle lithosphere  
 271 (ML) and topographic build-up  
 272

### 273 3.2 Uttarakhand Himalaya (UKH, 78-81°E longitude)

274 This region experienced notable earthquake events that include 1991 Uttarkashi earthquake  
 275 (M 6.7) and 1999 Chamoli earthquake (M 6.5). The entire Uttarakhand Himalaya is  
 276 associated with moderate  $k_{sn}$  values with a couple of localized high  $k_{sn}$  zones (Figure 2).  
 277 Interestingly, these anomalous high  $k_{sn}$  values are associated with the epicenters of the  
 278 1991 and 1999 earthquakes. The nature of  $k_{sn}$  pattern shows a NNE-SSW trend in the  
 279 western part of the Uttarakhand Himalaya to the north of the MCT (Figure 2). We infer that  
 280 this trend of the  $k_{sn}$  is an indication for extension of the DHR into the Higher Himalaya, which

281 is also supported by presence of rift-type morphology, (Kaurik-Chango rift) in the extreme  
282 north of the region (Arora et al., 2012) A recent seismological P-Receiver Function (P-RF) H-  
283 K stacking study (Mandal et al., 2021) has suggested the presence of three NS-to-NNE  
284 trending transverse structures beneath the Uttarakhand Himalaya characterized by  
285 significant Moho up-warp and large values (~1.85-2.13) of the ratio between the P- and the  
286 S-wave velocities. Manglik et al. (2022) suggested the extension of different litho-units of the  
287 Aravalli-Delhi Fold belt into the Delhi Seismic Zone and inferred their presence beneath the  
288 Uttarakhand Himalaya, leading to a spatially heterogeneous crust for this region. We  
289 therefore propose that the extension of DHR to the north of the MCT could represent the  
290 segment boundary that structurally divides the western Himalaya and the Uttarakhand  
291 Himalaya.

292 A study by Manglik et al. (2021) from the analysis of the basin width and the distance  
293 between the major thrusts (MFT and MCT) shows positive correlation in this part of the  
294 Himalaya. They considered this part of the Himalaya as one of the segments among the 5  
295 major segments of the collision belt. They further opined that the Great Boundary Fault in the  
296 eastern side of the Uttarakhand Himalaya possibly separates this from western Nepal. A  
297 northward shift in the  $k_{sn}$  pattern supports the disposition of the major thrust faults in this  
298 segment (Figure 2). Moderate values of the  $k_{sn}$  suggest comparably strong IML with respect  
299 to western Himalaya, having low dip angle of the Indian plate, but high in comparison to the  
300 western Himalaya. We infer that in this segment of the Himalaya also, the IML extends to  
301 further north but not as much as it is in the western Himalaya. Zhao et al. (2010) have shown  
302 that the Indian plate subduction in this segment is getting steeper and reaches far north,  
303 almost to the Tarim Basin.

### 304 **3.3 Western Nepal Himalaya (WNH, 81 - 83°E longitude)**

305 We observe a lateral shift in the  $k_{sn}$  pattern (81.5-82.7°E) (Figure 2) which is correlating well  
306 with the previously inferred transverse faults of the western Nepal fault system (WNFS).  
307 Seismicity pattern is also well collaborating with this shift in the  $k_{sn}$  pattern where a cluster of  
308 earthquakes are concentrated in this zone (Figure 1). Faizabad ridge, one of the structurally  
309 important transverse ridges in the Ganga foreland basin, is located towards the eastern end  
310 of the region. Manglik et al. (2021) have shown negative and positive correlation in the basin  
311 width and relative displacement of MCT and MFT on either side, respectively, of the  
312 projection of the FR into the Himalaya and suggested a segment boundary in this region.  
313 However, magnetotelluric results of Demudu Babu et al. (2020) preclude northward

314 extension of the present inferred shape of the FR. They suggested that the FR, if present  
315 beneath the Himalaya, might have deviated from its present inferred position.

316

317 The  $k_{sn}$  values observed in this segment of the Himalaya is relatively high compared to  
318 the western and Uttarakhand Himalaya, which is mostly confined to northernmost region  
319 suggesting a weaker IML and steep angle of underthrusting for this region compared to that  
320 in the western Himalaya and Uttarakhand. Harvey et al. (2015) studied along-arc  
321 topographic discontinuities with the help of  $k_{sn}$  and seismicity distribution in the central  
322 Himalaya and proposed a tectonic boundary in this segment (82.5°E) with a steep (50°)  
323 ramp in the MHT beneath western Nepal. They also opined that the occurrence of recent  
324 tectonic activity in this zone is causing the rise in topography. Another study by Murphy et al.  
325 (2014) came up with the presence of western Nepal Fault System (WNFS) that likely serves  
326 as a demarcating boundary of the strain-segregated region of the WNH which contains a  
327 first-order structure in the 3D displacement field of the WNH range. Cannon and Murphy  
328 (2014) inferred that the seismotectonic model of the Central Nepal is not the same in the  
329 case of WNH as the formers model is relatively simple, whereas, the latter's model is  
330 complicated in terms of regional geology, micro-seismicity and other factors indicate  
331 evidence for structural duplexing underneath the lesser and higher Himalaya. However,  
332 contrary to this Subedi et al. (2018) inferred that the Moho in the WNH is mildly dipping north  
333 at about 40 km under the foothills to about 58 km below the Higher Himalaya and increase  
334 underneath the southern Tibet. They advised that the crustal structure of WNH is identical to  
335 that of the Central Nepal and Garhwal Himalaya of the Uttarakhand region.

336 Previous geophysical studies suggested that geometry of the MHT is laterally varying.  
337 Larson et al. (1999) and Van der Beek et al. (2002) suggested that the southern flat ramp of  
338 the MHT is relatively steep compared to that in the central Nepal. However, the dip of the  
339 mid-crustal MHT ramp is much steeper in central Nepal rather than the WNH (Berger et al.,  
340 2004). From the observed pattern of the  $k_{sn}$  and available geophysical data, we propose that  
341 the western Nepal Himalaya, lying west of the Faizabad ridge and east of the GBF,  
342 constitutes one of the segments of the Himalaya with relatively weak, relatively steeply  
343 dipping Indian lithosphere. One of the tearing boundaries of the Indian lithosphere proposed  
344 by Li and Song (2018) also coincides with this segment.

#### 345 **3.4 Central and Eastern Nepal Himalaya (83-88°E longitude)**

346 The central Nepal Himalaya is characterized by high to very high  $k_{sn}$  values where this  
347 region experienced 1984 Bihar-Nepal earthquake (M 8.0) and very recent 2015 Gorkha  
348 earthquake (M 7.8). The location of the 2015 earthquake is associated with a zone of high

349  $k_{sn}$  (Figure 2). There are several patches of high  $k_{sn}$  values observed in this zone which  
350 could be due to various transverse tectonic features existing in the region, e.g. Judi  
351 lineament, Gourishankar lineament (Mugnier et al., 2017). The high  $k_{sn}$  values observed in  
352 this zone suggest weaker part of the IML and steep dip angle of the Indian lithosphere.  
353 Manglik et al. (2021) has shown positive correlation of the basin width and relative  
354 separation of the major thrust sheets. Results from previous studies also support the less  
355 northward extent of the IML compared to that in the western Himalaya (Figure 2).

### 356 **3.5 Sikkim and western Bhutan Himalaya (88-89°E longitude)**

357 The  $k_{sn}$  pattern shows a prominent NNW-SSE trending linear high zone in this segment  
358 (Figure 2). This zone is prevailed by strike-slip deformation and deep crustal earthquakes on  
359 the planes oblique to the northward convergence of the Indian plate (Drukpa et al., 2006;  
360 Hazarika et al., 2010; Pavankumar et al., 2014; Paul and Mitra, 2015; Diehl et al., 2017;  
361 Pavankumar and Manglik, 2021). The Sikkim earthquake (Mw 6.9) of September 18, 2011  
362 with the focal depth of 50 km (U.S Geological Survey (USGS); Ravi Kumar et al., 2012) is an  
363 example of such oblique deformation. Recent seismological and gravity studies carried out in  
364 the eastern segment of the Himalayan collision belt and adjoining foreland basin (Singer et  
365 al., 2017; Diehl et al., 2017; Grujic et al., 2018; Priestley, 2019) have recommended a NW-  
366 SE trending mid-crustal fault zone, termed as the Dhubri–Chungthang fault (DCF) extending  
367 from Chungthang locality in northeast Sikkim to Dhubri locality at the north-western edge of  
368 the Shillong Plateau that possibly breaks the Indian plate and the MHT underneath the  
369 eastern Himalaya. Pavankumar and Manglik (2021) using the broadband and long period  
370 magnetotelluric investigations suggested a NW-SE trending lithospheric-scale seismogenic  
371 fault that separates two geologically and compositionally distinct blocks of the Indian plate  
372 underthrusting the Himalaya beneath the MCTZ. It can be seen that the  $k_{sn}$  trend coincides  
373 with the NNW-SSE Dhubri-Chunthang fault (DCF). Geophysical studies suggested that the  
374 structure of the underthrusting Indian lithosphere under the Sikkim Himalaya acts as a major  
375 factor responsible in dividing along-strike convergence across the Eastern Himalaya

376 A significant distinction in the structure of the Moho and the MHT in the Bhutan Himalaya  
377 has been ascertained from the receiver function analysis by Singer et al. (2017) which is  
378 also reflected in the  $k_{sn}$  patterns of the western and Eastern Bhutan. It is interesting to note  
379 that, although, the northern part of the western Himalaya is associated with the low to  
380 moderate  $k_{sn}$ , the Moho geometry shown by Singer et al. (2017) inferred an increased dip of  
381 the Moho south of the Higher Himalaya spreading almost 70 km depth, however, in eastern  
382 Bhutan the Moho is nearly sub-horizontal at 50 km depth. Contrary to this, Robert et al.

383 (2011) suggested the absence of crustal-scale MHT ramp in western Bhutan whereas  
384 increase in the dip of the mid-crustal ramp of the MHT in central Nepal. Previously, Hauck et  
385 al. (1998) inferred that westernmost Bhutan represents a changeover zone amidst the  
386 Bhutan and Nepal Himalaya which could be linked with the DCF. We therefore propose that  
387 the NW-SE trending DCF could be an active tectonic boundary that might separate the  
388 Sikkim and western Bhutan segment with the eastern Bhutan, similar to the GBF that  
389 possibly separates the Uttarakhand Himalaya with the western Nepal Himalaya.

### 390 **3.6 Along arc-variations of the $k_{sn}$ and its relation with the extent of IML**

391 We attempted to see any qualitative relation between the  $k_{sn}$  pattern with the extent of Indian  
392 mantle lithosphere beneath the Tibetan plateau. We have plotted the northern extent of the  
393 Indian mantle lithosphere proposed by various researchers on Figure 2. Except Li and Song  
394 (2018), there is a gradual eastward decrease in the extent of the IML, suggesting the  
395 eastward decrease in the strength of the Indian lithosphere and increase in flexural bending  
396 beneath the Himalaya (Figure 2). This trend correlates well with the observed  $k_{sn}$  pattern.  
397 The Major tectonic/segmentation boundaries proposed from the present study, like DHR,  
398 GBF and DCF has good correlation with the Tears (T1, T2, T3), inferred from the velocity  
399 structure (Li and Song, 2018).

400 The logic behind varying geometries of the IML underneath the Tibet region might be  
401 associated with its intrinsic heterogeneity in its physical characteristics (Yin and Harrison,  
402 2000) or may be due to the heterogeneities of the physical properties of the Asian  
403 Continental lithosphere along the collision zone (Chen et al., 2017). The heterogenous  
404 progression of the DHR, GBF, DCF etc., may have subjected the IML to tear near the  
405 already-existing feeble zones while its northward movement. This contrast between the  
406 moving slabs can be augmented by the positive correlation between the dip angle and the  
407 rollback velocity of the slab. This model is persistent with the previous works which inferred  
408 that the IML is underthrusting below the southern Tibet with a gradual increase in dip  
409 towards east (Chen et al., 2015; Li et al., 2008; Zhao et al., 2010). This is further supported  
410 by the most recent Pn tomography study (Li and Song, 2018), where a significant tearing is  
411 observed apparently at the same position.

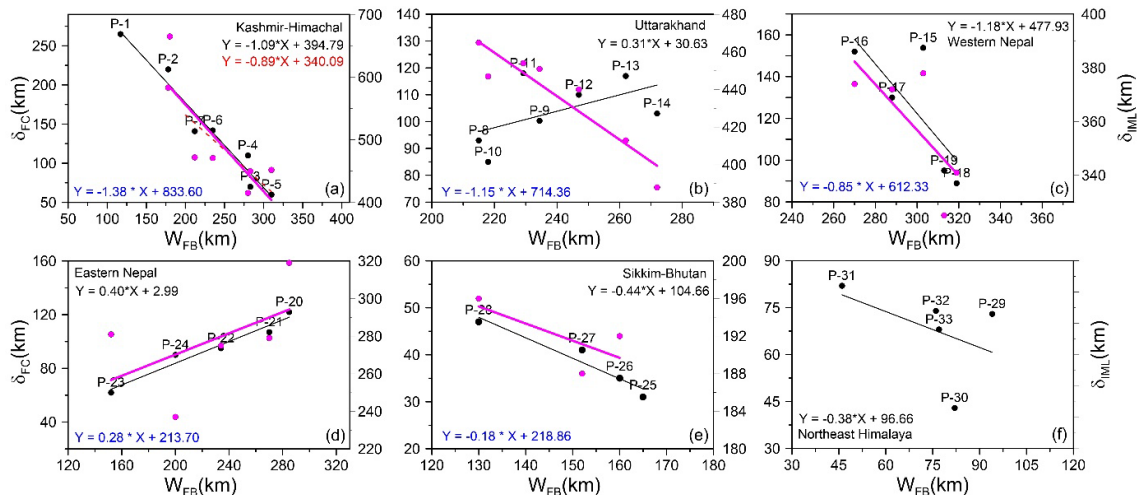
412 From the results of the Pn tomography, the IML which was subjected to subduction is torn  
413 into pieces that are subducting at varying dip angles, in this due process, the northern limits  
414 of the IML became shallower, thereby extending further towards west and east with a gentle  
415 dip and getting steeper in the middle extending up to the BNS (Li and Song, 2018) (Figure 2).  
416 Ravi Kumar et al. (2020) from their 2D-density modelling results suggested that the Indian

417 lithosphere subducts laterally up to the Karakoram at a gentle angle in the west. In the  
418 central part, a high angle of subduction is observed up until the south of the BNS, while  
419 towards east it subducts at a shallow angle nearing the ITSZ and possibly further south of  
420 the BNS.

421

### 422 **3.7 Width of the foreland basin and strength of the lithosphere**

423 We tried to establish a possible relationship between the width of the foreland basin and the  
424 northern extent of the Indian plate along the arc using the profiles published by Manglik et al.  
425 (2021) (Figure 4). Lateral variations in the geometry of a foreland basin are linked to  
426 changes in the mechanical characteristics of the plate carrying load which is a consequence  
427 from the past tectonic events viz., rifting passive margin formation, as well as to changes in  
428 the loads introduced on it (Waschbusch and Royden, 1992; Millan et al., 1995). Since the  
429 estimated  $k_{sn}$  suggests lateral variations that infer the variations in the load imposed on the  
430 underthrusting Indian plate, we propose the variable nature of the geometry of the foreland  
431 basin also. As the structure of the foreland basin is controlled by the flexural rigidity which is  
432 controlled by strength of the Indian plate, we attempted to analyze any correlations in basin  
433 width and northern extent of the IML. We calculated the distance from the MFT to the IML  
434 proposed by Li et al. (2008) and plotted these values along with the distance between MFT  
435 and MCT against the distance between southern limit of the Indo-Gangetic Foreland basin to  
436 MFT as shown in Manglik et al. (2021). The relationship between these three parameters is  
437 shown in Figure 4. From the Figure 4, it can be seen that the width of the foreland basin and  
438 the northern extent of the IML is strongly correlated. Qualitative comparison between these  
439 two parameters also suggests segmentation of the Indian plate into different blocks. Major  
440 observation of our analysis is that for the Uttarakhand region, there is a negative correlation,  
441 which indeed infers along-strike segmentation of the foreland basin too (Figure 4). This  
442 segmentation might control the thickness and geometry of sedimentary sequences  
443 deposited in the foreland basin. Manglik et al. (2021, 2022) proposed the GBF of the  
444 Aravalli-Delhi Fold Belt as a major tectonic boundary segmenting the Indian plate between  
445 the Kumaun and the western Nepal sections of the Himalaya. It implies that the Indian plate  
446 underthrusting the Uttarakhand Himalaya should be more complex spatially than a simple  
447 horizontally layered crust-mantle architecture with bearing on the earthquake genesis for this  
448 segment of the Himalaya.

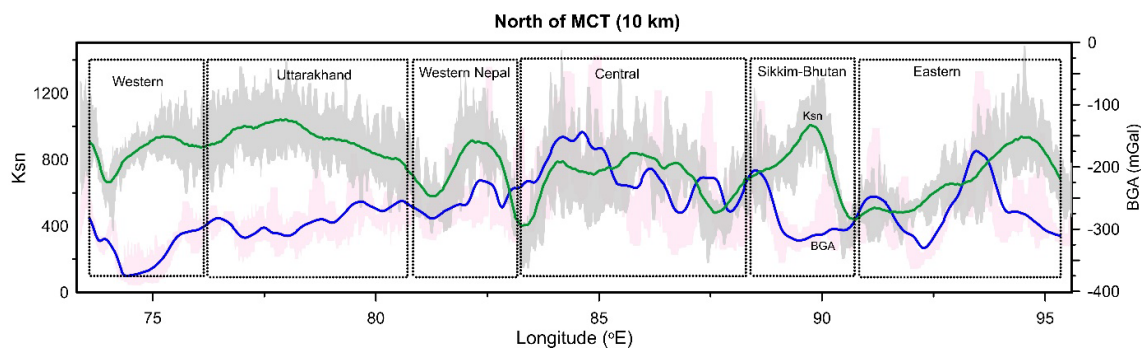


449

450 **Figure 4.** Relation between the width of the foreland basin ( $W_{FB}$ ) and the extent of the Indian  
 451 Mantle lithosphere (IML) from the Himalayan front (MFT) ( $\delta_{IML}$ ) [magenta colour line and  
 452 dots] for the segments of the Himalayan arc proposed by Manglik et al. (2021). The black  
 453 dots and lines are the relationship obtained by Manglik et al. (2021) between the  $W_{FB}$  and  
 454 segment length between the MFT and MCT ( $\delta_{FC}$ ).

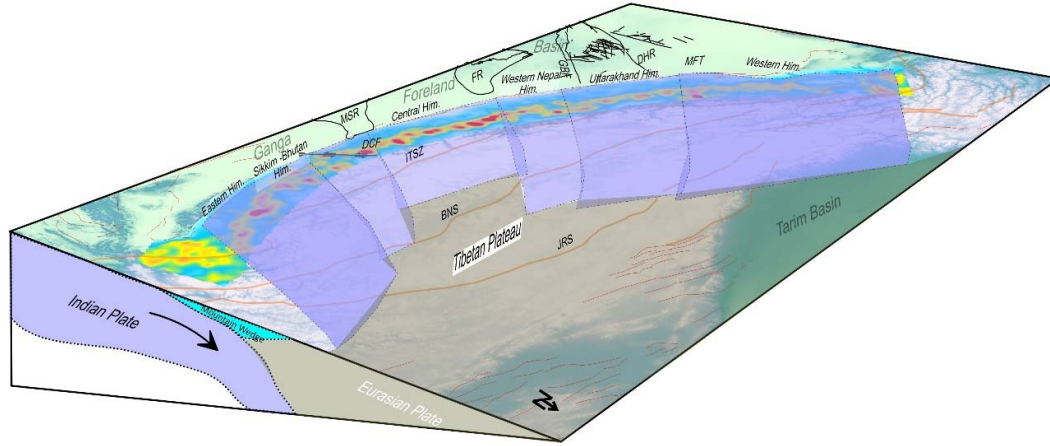
455

456 To analyse possible relationship between the  $k_{sn}$  and the Bouguer Gravity Anomalies  
 457 (BGA), we have plotted the longitude-wise variations of  $k_{sn}$  and BGA along the MCT towards  
 458 north with a swath of 10 km. The comparisons of these two parameters are shown in Figure  
 459 5. The trend of  $k_{sn}$  north of the MCT shows both positive and negative correlations. In  
 460 sectors like western Himalaya and western Nepal, the trend shows good positive correlation  
 461 whereas in parts of Uttarakhand and Sikkim-Bhutan segment it shows strong negative  
 462 correlation (Figure 5). We infer that there is a relationship between  $k_{sn}$  and structural  
 463 variations of individual segments. Manglik et al. (2021) have analysed 33 swath profiles of  
 464 BGA cutting across the arc which displayed a significant along-arc variations as well as a  
 465 change in its pattern across the foreland basin. They proposed that the lateral changes in  
 466 the fabric of Indian plate could be responsible for these variations. Further, a cartoon  
 467 depicting the segmentation boundaries are given in Figure 6.



468

469 **Figure 5:** A comparison of longitudinal variations of the  $k_{sn}$  with the BGA. The red line  
 470 indicates variations in  $k_{sn}$  and the blue line indicates variations in BGA. The profiles are  
 471 taken with a swath width of 10 kms from the MCT.  
 472



473  
 474  
 475 **Figure 6:** A Cartoon showing the segmented blocks of the Indian mantle lithosphere inferred  
 476 from the present study.

#### 477 **4. Conclusions**

478 Analysis of the normalized steepness Index computed for the Himalayan arc suggests  
 479 prominent along-arc variations and has strong correlation with the strength of the Indian  
 480 plate. By integrating the  $k_{sn}$  variations with the available geophysical information, we  
 481 correlated the segmented nature of the underthrusting Indian plate with other studies and  
 482 confirmed the presence of five major blocks. Various transverse tectonic features viz., the  
 483 Delhi-Haridwar Ridge, the Great Boundary Fault, and the Dhubri-Chungthang Faults are  
 484 inferred to be segmentation boundaries. Hence, we conclude that the  $k_{sn}$  index can be used  
 485 as a proxy to detect the segmentations in large scale tectonically active regions. A  
 486 comparison of the foreland width with the northern limit of the Indian plate suggests  
 487 segmented nature of the Ganga foreland basin with a significant variation in the Uttarakhand  
 488 Himalaya. We propose the inherent structural heterogeneities within the Indian plate might  
 489 be a possible reason for these segmentations. A detailed geophysical study to image three-  
 490 dimensional lithospheric architecture of the plate including the Ganga foreland basin is  
 491 necessary for better understanding of the geodynamic evolution of the Himalaya and robust  
 492 estimates of the seismic potential of the collision belt.

## 493 Acknowledgements

494 The study has been carried out under the project MLP-FBR0003-28(AM) sponsored by  
495 Council of Scientific and Industrial Research (CSIR). KRS acknowledges the project for a  
496 post-doc fellowship. The work has been approved by CSIR-National Geophysical Research  
497 Institute (CSIR-NGRI) for publication as contribution number NGRI/Lib/2022/Pub-xxx under  
498 the project MLP6404-28(AM).

499

## 500 Data Availability Statement

501 The Digital Elevation Model data that was used in this study can be downloaded from the  
502 following link <https://www.eorc.jaxa.jp/ALOS/en/aw3d30/index.htm>.

## 503 References:

- 504 1. Acton, C., Priestley, K., Mitra, S. & Gaur, V. (2011). Crustal structure of the Darjeeling—  
505 Sikkim Himalaya and southern Tibet. *Geophys. J. Int.* 184, 829–852.
- 506 2. Arora, B.R., Gahalaut, V.K. and Naresh, K. (2012). Structural control on along-strike variation  
507 in the seismicity of the northwest Himalaya. *Jour. Asian Earth Sci.*, v.57, pp.15–24.
- 508 3. Avouac, J. P. 2003. Mountain building, erosion and the seismic cycle in the Nepal Himalaya.  
509 *Advances in Geophysics* 46,1-80.
- 510 4. Demudu Babu, M., Manglik, A., Thiagarajan, S., Suresh, M. (2020). Electrical resistivity image  
511 of a basement ridge in the foreland central Ganga basin. *Journal of Applied Geophysics*, 179.  
512 <https://doi.org/10.1016/j.jappgeo.2020.104097>.
- 513 5. Bai L., Klemperer, S.L., Mori, J., Karplus, M.S., Ding, L., Liu, H., Li, G., Song, B. and Dhakal,  
514 S. (2019). Lateral variation of the Main Himalayan Thrust controls the rupture length of the  
515 2015 Gorkha earthquake in Nepal. *Sci. Adv.*, 5, eaav0723, doi: 10.1126/sciadv. aav0723.
- 516 6. Berger, A., Jouanne, F., Hassani, R. and Mugnier, J.L. (2004). Modelling the spatial distribution  
517 of present-day deformation in Nepal: how cylindrical is the Main Himalayan Thrust in Nepal?.  
518 *Geophysical Journal International*, 156: 94-114. [https://doi.org/10.1111/j.1365-  
519 246X.2004.02038.x](https://doi.org/10.1111/j.1365-246X.2004.02038.x).
- 520 7. Berthet, T., Ritz, J.-F., Ferry, M., Pelgay, P., Cattin, R., Drukpa, D., Braucher, R., Hetényi, G.  
521 (2014). Active tectonics of the eastern Himalaya: New constraints from the first tectonic  
522 geomorphology study in southern Bhutan. *Geology*, 42(5), 427–430.
- 523 8. Bilham, R. (2019). Himalayan earthquakes: a review of historical seismicity and early 21st  
524 century slip potential. *Geol. Soc. Lond. Spec. Publ.* 483(1):423–482.
- 525 9. Bilham, R., Blume, F., Bendick, R. and Gaur, V. K. (1998). Geodetic constraints on the  
526 translation and deformation of India: implications for future great Himalayan earthquakes.  
527 *Current Science*, 74, 213-229.
- 528 10. Boulton, S.J. and Stokes, M. (2018). Which DEM is best for analyzing fluvial landscape  
529 development in mountainous terrains? *Geomorphology*, 310, pp.168–187.
- 530 11. Brown, L.D. Zhao, W., Nelson, K.D., Hauck, M., Alsdorf, D., Ross, A., Cogan, M., Clark, M.,  
531 Liu, X., Che, J. (1996). Bright spots, structure, and magmatism in southern Tibet from  
532 INDEPTH seismic reflection profiling. *Science*, 274, 1688–1690.
- 533 12. Burov, E., and Diament, M. (1995). The effective elastic thickness ( $T_e$ ) of continental  
534 lithosphere: What does it really mean? *J. Geophys. Res.*, 100, 3905– 3927.

- 535 13. Caldwell, W. B., Klemperer, S.L., Lawrence, S.F., Rai, S.S., Ashish. (2013). Characterizing the  
536 Main Himalayan Thrust in the Garhwal Himalaya, India with receiver function CCP stacking.  
537 *Earth and Planetary Science Letters*, 367, 15-27.
- 538 14. Cannon, J., & Murphy, M. (2014). Active lower crustal deformation and Himalayan seismic  
539 hazard revealed by stream channels and regional geology. *Tectonophysics*, 633.  
540 10.1016/j.tecto.2014.06.031.
- 541 15. Chen, B., Liu, J., Chen, C., Du, J., & Sun, Y. (2015). Elastic thickness of the Himalayan-  
542 Tibetan orogen estimated from the fan wavelet coherence method, and its implications for  
543 lithospheric structure. *Earth and Planetary Science Letters*, 409, 1–14.  
544 <https://doi.org/10.1016/j.epsl.2014.10.039>.
- 545 16. Chen, M., Niu, F., Tromp, J., Lenardic, A., Lee, C. T. A., Cao, W., & Ribeiro, J. (2017).  
546 Lithospheric foundering and under thrusting imaged beneath Tibet. *Nature Communications*,  
547 8(1), 15659. <https://doi.org/10.1038/ncomms15659>.
- 548 17. Dahlen, F. A., (1990). Critical taper model of fold-and-thrust belts and accretionary wedges.  
549 *Annual Review of Earth and Planetary Science*, 18, 55–99,  
550 doi:10.1146/annurev.ea.18.050190.000415.
- 551 18. Dal Zilio, L., Hetényi, G., Hubbard, J. and Bollinger, L. (2021). Building the Himalaya from  
552 tectonic to earthquake scales. *Nat. Rev. Earth Environ.*, 2, pp.251–268.
- 553 19. Dal Zilio, L., Jolivet, R., Van Dinther, Y. (2020). Segmentation of the Main Himalayan Thrust  
554 illuminated by Bayesian inference of interseismic coupling. *Geophys. Res. Lett.* 47(4):  
555 e2019GL086424.
- 556 20. Diehl, T., Singer, J., Hetényi, G., Grujic, D., Clinton, J., Giardini, D., Kissling, E., Group, G.W.  
557 (2017). Seismotectonics of Bhutan: evidence for segmentation of the Eastern Himalayas and  
558 link to foreland deformation. *Earth Planet. Sci. Lett.*, 471, pp. 54-64.
- 559 21. Drukpa, D., Velasco, A., Doser, D. (2006). Seismicity in the Kingdom of Bhutan (1937–2003):  
560 Evidence for crustal transcurrent deformation. *Journal of Geophysical Research*, 111.  
561 10.1029/2004JB003087.
- 562 22. Elliott, J.R., Jolivet, R., González, P.J., Avouac, J., Hollingsworth, J. and Searle, M.P. (2016).  
563 Himalayan megathrust geometry and relation to topography revealed by the Gorkha earthquake.  
564 *Nature Geosci.*, 9, pp.174–180.
- 565 23. Ghavri, S., Jade, S. (2021). Seismic potential of megathrust in the Kumaun-Garhwal region of  
566 NW Himalaya: implications from geodetic and seismic strain rates. *International Journal of*  
567 *Earth Sciences*. 110:1439–1452. <https://doi.org/10.1007/s00531-021-02023-x>.
- 568 24. Godin, L., La Roche, R.S., Waffle, L. and Harris, L.B. (2018). Influence of inherited Indian  
569 basement faults on the evolution of the Himalayan Orogen. *Geological Society, London,*  
570 *Special Publications*, 481, pp. 251 – 276, <https://doi.org/10.1144/SP481.4>.
- 571 25. Grujic, D., Hetényi, G., Cattin, R., Baruah, S., Benoit, A., Drukpa, D., Saric, Adi. (2018). Stress  
572 transfer and connectivity between the Bhutan Himalaya and the Shillong Plateau.  
573 *Tectonophysics*, 744. 322-332. 10.1016/j.tecto.2018.07.018.
- 574 26. Hammer, P., Berthet, T., Hetényi, G., Cattin, R., Drukpa, D., Chopel, J., Lechmann, S.,  
575 Moigne, N. Le, Champollion, C., and Doerflinger, E. (2013). Flexure of the India plate  
576 underneath the Bhutan Himalaya. *Geophys. Res. Lett.*, 40, 4225- 4230. doi:10.1002/grl.50793.
- 577 27. Hammer, P., Berthet, T., Hetényi, G., Cattin, R., Drukpa, D., Chopel, J., Lechmann S., Le  
578 Moigne, N., Champollion, C., and Doerflinger, E. (2013). Flexure of the India plate underneath  
579 the Bhutan Himalaya. *Geophys. Res. Lett.*, 40 pp: 4225–4230, doi:10.1002/grl.50793.
- 580 28. Han, Z., Li, X., Wang, N., Chen, G., Wang, X., Lu, H. (2017). Application of river longitudinal  
581 profile morphometrics to reveal the uplift of Lushan Mountain. *Acta Geologica Sinica- English*  
582 *Edition*, 91 (5), 1644–1652.

- 583 29. Harvey, J., Burbank, D., Bookhagen, B. (2015). Along-strike changes in Himalayan thrust  
584 geometry: Topographic and tectonic discontinuities in western Nepal. *Lithosphere*, 7.  
585 10.1130/L444.1.
- 586 30. Hauck, M. L., Nelson, K. D., Brown, L. D., Zhao, W., Ross, A. R. (1998). Crustal structure of  
587 the Himalayan orogen at ~90° east longitude from Project INDEPTH deep seismic reflection  
588 profiles. *Tectonics*, 17, 481– 500, doi:10.1029/98TC01314.
- 589 31. Hazarika, P., Kumar, M., Gudhimella, S., Raju, P., Rao, N., Srinagesh, D. (2010). Transverse  
590 Tectonics in the Sikkim Himalaya: Evidence from Seismicity and Focal-Mechanism Data.  
591 *Bulletin of The Seismological Society of America*, 100. 1816-1822. 10.1785/0120090339.
- 592 32. Hetényi, G., Cattin, R., Berthet T., Le Moigne, N., Chopel, J., Lechmann, S., Hammer, P.,  
593 Drukpa, D., Sapkota, S.N., Gautier, S. and Thinley, K. (2016). Segmentation of the Himalayas  
594 as revealed by arc-parallel gravity anomalies. *Sci. Rep.*, 6, 33866.
- 595 33. Hetényi, G., Cattin, R., Vergne, J., and Nábèlek, J.L., (2006). The effective elastic thickness of  
596 the India Plate from receiver function imaging, gravity anomalies and thermomechanical  
597 modelling, *Geophys. J. Int.*, 167, pp: 1106–1118, doi:10.1111/j.1365-246X.2006.03198.x.
- 598 34. Howard, A.D. (1998). Long profile development of bedrock channels, Interaction of  
599 weathering, mass wasting, bed erosion, and sediment transport. *Geophysical Monograph*  
600 *American Geophysical Union*. 107, 297–319.
- 601 35. Howard, A.D., Kirby, G. (1983). Channel changes in badlands. *Geol. Soc. Am. Bull.* 94, 739–  
602 752.
- 603 36. Jade, S. (2004). Estimates of plate velocity and crustal deformation in the Indian subcontinent  
604 using GPS geodesy. *Current Science*, 86, 1343-1348.
- 605 37. Jordan, T.A., and Watts, A.B. (2005). Gravity anomalies, flexure and the elastic thickness  
606 structure of the India–Eurasia collisional system. *Earth Planet. Sci. Lett.*, 236, pp: 732–750.
- 607 38. Kirby, E., Whipple, K, X. (2012). Expression of active tectonics in erosional landscapes.  
608 *Journal of Structural Geology*, 44, 54-75.
- 609 39. Kosarev, G., Kind, R., Sobolev, S.V., Yuan, X., Hanka, W., Oreshin, S. (1999). Seismic  
610 evidence for detached Indian lithospheric mantle beneath central Tibet. *Science*, 283, 1306–  
611 1308.
- 612 40. Lague, D. (2013). The stream power river incision model, evidence, theory and beyond. *Earth*  
613 *Surf. Process. Landforms* 39 (1), 38–61.
- 614 41. Larson, K., Burgmann, R., Bilham, R., Freymuller, J. (1999). Kinematics of the India-Eurasia  
615 collision Zone from GPS measurements. *Journal of Geophysical Research: Solid Earth*, 104.  
616 10.1029/1998JB900043.
- 617 42. Li, C., Hilst, R.D.V.D., Meltzer, A.S., Engdahl, E.R. (2008). Subduction of the Indian  
618 lithosphere beneath the Tibetan Plateau and Burma. *Earth Planet. Sci. Lett.*, 274, pp. 157-168.
- 619 43. Li, J. and Song, X. (2018). Tearing of Indian mantle lithosphere from high-resolution seismic  
620 images and its implications for lithosphere coupling in southern Tibet. *Proc. Natl. Acad. Sci.*,  
621 115, pp.8296-8300.
- 622 44. Liang, X., & Sandvol, Eric & Chen, Youqiang & Hearn, Thomas & Ni, James & Klempere,  
623 Simon & Shen, Yang & Tilmann, Frederik. (2012). A fragmented Indian slab and no south-  
624 verging subduction. *Earth and Planetary Science Letters*, 333-334. 101-111.
- 625 45. Liang, X., Shen, Y., Chen, J., Ren, Y. (2007). Crustal and mantle velocity models of southern  
626 Tibet from finite frequency tomography. *Journal of Geophysical Research: Solid Earth*, 116,  
627 10.1029/2009JB007159.

- 628 46. Lyon-Caen, H. & Molnar, P. (1985). Constraints on the structure of the Himalaya from an  
629 analysis of gravity anomalies and a flexural model of the lithosphere. *J. Geophys. Res. Solid*  
630 *Earth*, 88, 8171–8191.
- 631 47. Mahesh, P., Rai, S., Sivaram, K., Paul, A., Gupta, S., Sarma, R., Gaur, V. (2013). One-  
632 dimensional reference velocity model and precise locations of earthquake hypocenters in the  
633 Kumaon-Garhwal Himalaya. *Bulletin of the Seismological Society of America*, 103(1), 328–  
634 339.
- 635 48. Mandal, N., Bose, S., Baruah, A., Sarkar, S. (2015). First-order topography of the Himalayan  
636 Mountain belt: A deep-crustal flow analysis. *Geological Society, London, Special Publications*,  
637 412. 10.1144/SP412.9.
- 638 49. Manglik, A., Kandregula, R.S., Gayatri, P.K. (2022). Foreland Basin Geometry and Disposition  
639 of Major Thrust Faults as Proxies for Identification of Segmentation along the Himalayan Arc.  
640 *Journal of the Geological Society of India*, 98, 57-61. [https://doi.org/10.1007/s12594-022-1928-](https://doi.org/10.1007/s12594-022-1928-y)  
641 [y](https://doi.org/10.1007/s12594-022-1928-y).
- 642 50. McNutt, M., Diament, M., Kogan, M. (1988). Variations of Elastic Plate Thickness at  
643 Continental Thrust Belts. *Journal of Geophysical Research*, 93. 8825-8838.  
644 10.1029/JB093iB08p08825.
- 645 51. Molnar, P. and Lyon Caen, H. (1989). Fault-plane solutions of earthquakes and active tectonics  
646 of the Tibetan plateau and its margins. *Geophysical Journal International*, 99, 123–153.
- 647 52. Molnar, P. and Tapponnier, P. (1975). Cenozoic tectonics of Asia: effects of a continental  
648 collision. *Science*, 189, 419-426.
- 649 53. Mugnier, Jean-Louis., Jouanne, F., Bhattarai, R., Cortés-Aranda, J., Gajurel, A., Leturmy, P.,  
650 Robert, X., Upreti, B., Vassallo, R. (2017). Segmentation of the Himalayan megathrust around  
651 the Gorkha earthquake (25 April 2015) in Nepal. *Journal of Asian Earth Sciences*, 141.  
652 10.1016/j.jseas.2017.01.015.
- 653 54. Murodov, D., Mi, W., Murodov, A., Oimuhmmadzoda, I., Abdulov S., Xin W. (2022). Deep  
654 Crustal Structure Beneath the Pamir–Tibetan Plateau: Insights from the Moho Depth and Vp/Vs  
655 Ratio Variation. *Frontiers in Earth Science*, 10.103389/feart.2022.821497.
- 656 55. Murphy, M., Taylor, M., Gosse, J., Silver, C., Whipp, D., Beaumont, C. (2014). Limit of strain  
657 partitioning in the Himalaya marked by large earthquakes in western Nepal. *Nature Geoscience*.  
658 7, 38. 10.1038/ngeo2017.
- 659 56. Nábělek, J., G. Hetényi, J. Vergne, S. Sapkota, B. Kafle, M. Jiang, H. Su, J. Chen, B. Huang,  
660 and the Hi-CLIMB Team. (2009). Underplating in the Himalaya-Tibet collision zone revealed  
661 by the Hi-CLIMB experiment. *Science*, 325, 1371–1374, doi:10.1126/science.1167719.
- 662 57. Nelson, K.D., Zhao, W., Brown, L.D., Kuo, J., Che, J. (1996). Partially molten middle crust  
663 beneath southern Tibet: synthesis of project INDEPTH results. *Science*, 274, pp. 1684-1688,  
664 10.1126/science.274.5293.1684.
- 665 58. Parsons, A. J., Hosseini, K., Palin, R. M., Sigloch, K. (2020). Geological, geophysical and plate  
666 kinematic constraints for models of the India-Asia collision and the post-Triassic central Tethys  
667 oceans. *Earth-Science Reviews*, 208, 103084. <https://doi.org/10.1016/j.earscirev.2020.103084>
- 668 59. Patriat, P. and Achache, J. (1984). India–Eurasia collision chronology has implications for  
669 crustal shortening and driving mechanism of plates. *Nature*, 311, 615–621.
- 670 60. Paul, H., Mitra, S., Bhattacharya, S., Suresh, G. (2015). Active transverse faulting within  
671 underthrust Indian crust beneath the Sikkim Himalaya. *Geophys. J. Int.*, 201., pp. 1072-1083.
- 672 61. Pavankumar, G., Manglik, A., (2021). Complex tectonic setting and deep crustal seismicity of  
673 the Sikkim Himalaya: An electrical resistivity perspective. *Physics and Chemistry of the Earth,*  
674 *Parts A/B/C*, 124(2). <https://doi.org/10.1016/j.pce.2021.103077>.

- 675 62. Pavankumar, G., Manglik, A., Thiagarajan, S. (2014). Crustal geoelectric structure of the  
676 Sikkim Himalaya and adjoining Gangetic foreland basin. *Tectonophysics*, 637, 238-250.  
677 <https://doi.org/10.1016/j.tecto.2014.10.009>.
- 678 63. Priestley, K., Ho, T., and Mitra, S. (2019). The Crustal Structure of the Himalaya: A Synthesis.  
679 *Geol. Soc. Lond. Spec. Publications* 483, 483–516. doi:10.1144/SP483-2018-127.
- 680 64. Rajendran, C.P., Rajendran, K. (2005). The status of central seismic gap: a perspective based on  
681 the spatial and temporal aspects of the large Himalayan earthquakes. *Tectonophysics*, 395:19–  
682 39.
- 683 65. Ravi Kumar, M., Hazarika, P., Prasad, G.S., Singh, A., Saha, S. (2012). Tectonic implications  
684 of the September 2011 Sikkim earthquake and its aftershocks. *Curr Sci*. 102:788–792.
- 685 66. Ravi Kumar, M., Singh, B., Pavan Kumar, V., Satyakumar, A. V., Ramesh, D. S., & Tiwari, V.  
686 M. (2020). Lithospheric density structure and effective elastic thickness beneath Himalaya and  
687 Tibetan plateau: Inference from the integrated analysis of gravity, geoid, and topographic data  
688 incorporating seismic constraints. *Tectonics*, 39, e2020TC006219.  
689 <https://doi.org/10.1029/2020TC006219>
- 690 67. Robert, X., Van der Beek P., Braun J., Perry C., Mugnier J.L. (2011). Control of detachment  
691 geometry on lateral variations in exhumation rates in the Himalaya: insights from low-  
692 temperature thermochronology and numerical modelling. *J. geophys. Res.*, 116, pg. B05202,  
693 doi:10.1029/2010JB007893.
- 694 68. Royden, L, Perron, J.T. (2012). Solutions of the stream power equation and application to the  
695 evolution of river longitudinal profiles. *Journal of Geophysical Research Earth Surf*. 118 (2),  
696 497–518.
- 697 69. Schwanghart, W., Kuhn, N. J., (2010). TopoToolbox: A set of Matlab functions for topographic  
698 analysis. *Environmental Modelling & Software* 25(6), 770–781.
- 699 70. Schwanghart, W., Scherler, D. (2014). Short Communication: TopoToolbox 2 – MATLAB-  
700 based software for topographic analysis and modelling in Earth surface sciences. *Earth Surface*  
701 *Dynamics* 2(1), 1–7.
- 702 71. Shaokun Si., Gao, R., Tian, X. (2019). Eastwest differential under thrusting of the Indian  
703 lithospheric plate beneath central Tibet revealed by imaging VP/VS. *Journal of Geophysical*  
704 *Research: Solid Earth*, 124, 9714–9730. <https://doi.org/10.1029/2018JB017259>
- 705 72. Singer, J., Kissling, E., Diehl, T., Hetényi, G. (2017). The under thrusting Indian crust and its  
706 role in collision dynamics of the Eastern Himalaya in Bhutan: insights from receiver function  
707 imaging. *J. Geophys. Res. Solid Earth*, 122, pp. 1152-1178.
- 708 73. Snyder, N.P., Whipple, K.X., Tucker, G.E., Merrittis, D.J. (2000). Landscape response to  
709 tectonic forcing, Digital elevation model analysis of stream profiles in the Mendocino triple  
710 junction region, northern California. *GSA Bulletin* 112 (8), 1250–1263.
- 711 74. Subedi, S., Hetényi, G., Vergne, J., Bollinger, L., Lyon-Caen, H., Farra, V. (2018). Imaging the  
712 Moho and the Main Himalayan Thrust in Western Nepal with receiver functions. *Geophysical*  
713 *Research Letters*, 45, 13,222– 13,230. <https://doi.org/10.1029/2018GL080911>.
- 714 75. Tilmann, F., Ni, J. (2003). Seismic Imaging of the Downwelling Indian Lithosphere Beneath  
715 Central Tibet. *Science (New York, N.Y.)*. 300. 1424-7. 10.1126/science.1082777.
- 716 76. Tiwari, V. M., Vyghreswara Rao, M. B. S., Mishra, D. C., Singh, B. (2006). Crustal structure  
717 across Sikkim, NE Himalaya from new gravity and magnetic data. *Earth Planet. Sci. Lett.*, 247,  
718 61–69.
- 719 77. Tunini, L., Jiménez-Munt, I., Fernandez, M., Vergés, J., Villaseñor, A., Melchiorre, M., &  
720 Afonso, J. C. (2016). Geophysical-petrological model of the crust and upper mantle in the  
721 India-Eurasia collision zone. *Tectonics*, 35, 1642–1669. <https://doi.org/10.1002/2016TC004161>

- 722 78. Van der Beek, P., Champel, B., Mugnier, Jean-Louis. (2002). Controls on drainage  
723 development in regions of active fault-propagation folding. *Geology*, 30. 10.1130/0091-  
724 7613(2002)030<0471: CODDOD>2.0.CO;2.
- 725 79. Wang, Q., Zang, P., Freymueller, J. T., Bilham, R., Larson, K. M., Lai, X., You, X., Niu, Z.,  
726 Wu, J., Li, Y., Yang, Z., and Chen, Q. (2001). Present day crustal deformation in China  
727 constrained by Global Positioning System measurements. *Science*, 294, 574-577.
- 728 80. Whipple, K.X., Tucker, G.E. (2002). Implications of sediment-flux-dependent river incision  
729 models for landscape evolution. *Journal of Geophysical Research Solid Earth*. 107 (B2) ETG-  
730 3.
- 731 81. Wittlinger, G., Farra, V., Hetényi, G., Vergne, J., Nábělek, J. (2009). Seismic velocities in  
732 Southern Tibet lower crust: A receiver function approach for eclogite detection. *Geophys. J.*  
733 *Int.*, 177, 1037–1049, doi:10.1111/j.1365-246X.2008.04084. x.
- 734 82. Wobus, C., Whipple, K.X., Kirby, E., Snyder, N., Johnson, J., Spyropolou, K., Crosby, B.,  
735 Sheehan, D., Willett, S.D. (2006). Tectonics from topography, Procedures, promise, and  
736 pitfalls. *Spec. Pap. Geol. Soc. Am.* 398, 55.
- 737 83. Yin, A. (2006). Cenozoic tectonic evolution of the Himalayan orogen as constrained by along-  
738 strike variation of structural geometry exhumation history and foreland sedimentation. *Earth*  
739 *Sci. Rev.*, 71:1–131.
- 740 84. Yin, A., Harrison, T. (2000). Geologic Evolution of the Himalayan-Tibetan Orogen. *Annual*  
741 *Review of Earth and Planetary Sciences*, 28. 211-280. 10.1146/annurev.earth.28.1.211.
- 742 85. Zhang, P., Shen, Z., Wang, M., Gan, W., Burgmann, R., Molnar, P., Wang, Q., Niu, Z., Sun, J.,  
743 Wu, J., Hanrong, S. and Xinzhao, Y. (2004). Continuous deformation of the Tibetan Plateau  
744 from global positioning system data. *Geology*, 32 (9), 809-812.
- 745 86. Zhao, J., Yuan, X., Liu, H., Kumar, P., Pei, S., Kind, R., Zhang, Z., Teng, J., Ding, L., Gao, X.,  
746 Xu, Q. and Wang, W. (2010). The boundary between the Indian and Asian tectonic plates below  
747 Tibet. *Proc. Natl. Acad. Sci.*, 107, pp.11,229–11,233.
- 748 87. Zhao, W. J., K. D. Nelson, and Project INDEPTH Team (1993). Deep seismic reflection  
749 evidence for continental under thrusting beneath southern Tibet. *Nature*, 366, 557–559.

750

**X-X-X**